JETIR.ORG ISSN: 2349-5162 | ESTD Year : 2014 | Monthly Issue
JOURNAL OF EMERGING TECHNOLOGIES AND INNOVATIVE RESEARCH (JETIR)
An International Scholarly Open Access, Peer-reviewed, Refereed Journal

Low-cost method qualitatively verifying the role of blowing jets in improving airflow across airfoils experiencing flow separation

Harsh Mathur[1], *Adithya Narayanan*[2*]
[1]*Bishop Cotton's, Bengaluru, India*
[2]*Physics, Ecole Polytechnique, Palaiseau, France*
** E-mail: adithya.narayanan@polytechnique.edu*

Abstract: High angle of attack (α) conditions coupled with low relative airflow velocities result in sudden losses of upthrust, a fatal outcome of the induced turbulent flow. This project aims to closely study the separated flow over a wing section using a low cost method: observations were conducted in a self-fabricated open-circuit wind tunnel. A modified nozzle-jet over the wing surface tangentially blew over the surface to counter the destabilisation of the boundary layer. First, the conditions under which the separation of flow was visible in the effective chord length of the airfoil were noted. These conditions were controlled across the NACA 2412 airfoil and wind tunnel testing environment variables. The countering mechanism for the separation was activated under the same controlled parameters to test the effectiveness of the method.

The experimental verification draws plots from direct imagery captured from the windtunnel trials. Images of the opaque gas stream (airflow visualiser in the test section) of high α conditions were captured. Greyscale renders of the images highlighting the precise paths of the fluid were produced. We compared the two fluid distribution greyscales by plotting their positions on a 2D xy-plane. The cost effective method was able to demonstrate the effectiveness of the nozzle-jets.

1 Introduction

The practical design of aviation intermittently requires fixed-wing aircrafts to manoeuvre with high angles of attack (α) at low velocities. In these critical conditions, it is common to find separated airflow within the realm of the airfoil; this further causes the formation of eddies and turbulent vorticies, destabilising the boundary layer.

The tangential blowing removed the randomised fluid paths and induced certain laminarity. The simple graphing mechanism demonstrated the fluid particles that were turbulently spaced at high αconditions were removed upon the activation of synthetic jets.

The objective of this paper is to demonstrate the results of the effects of tangential blowing by utilising a low-cost method to show those results. The use of direct wind tunnel imagery in the process of verifying the impact of the blowing jets is a rare method to find in aerodynamics research. However, in this paper we reveal that the advantages of this method are derived from its simplicity. Circumventing the heavy requirements of computational fluid dynamics (CFD), the imagery method plots the bounding stream paths that reveals crucial details about the nature of the streamlines and general fluid flow. The works of You, Moin *et al* [1] and Pfingston and Rade-
spiel [2] reveal the direct correlation between wind tunnel imagery and quantitative parameters. The supporting theory explains why the effectiveness of the jets is as clearly visible as it is under the blowing conditions. The images demonstrate the induced severity of the separated flow caused by the adversity of the pressure gradient. These stagnation points were alleviated to a satisfactory extent by the blowing jet, which is supported by the same form of imagery produced from the experiment.

2 Flow separation

As the airfoil's α is 22.5°, a value higher than the tested stall angle for NACA 2412 from the data found in Prabhakar [3], a large amount of separation occurs. The separation occurs further than in general due to the onset of turbulence and the fact that turbulent boundary layers are much thicker than laminar ones. The understanding of pressure gradients and their strength would help in understanding if the jets can realistically eliminate flow separation.

The jet equations would modify the boundary layer ones: either making them laminar definitions or turbulent ones. Taking these points into consideration, we can split the understanding of flow separation into 3 parts - Boundary layer equations with blowing, transition to turbulence and the effect of the pressure gradient.

2.1 General equations of boundary layers and jets

We know some basic equations for laminar boundary layers (B.L.) referenced from Kundu *et al* [4]:

$$\frac{\partial u}{\partial x} + \frac{\partial v}{\partial y} = 0 \tag{1}$$

$$\frac{\partial u}{\partial t} + y\frac{\partial u}{\partial x} + v\frac{\partial v}{\partial y} = \frac{1}{\rho}\frac{\partial \tau}{\partial y} \tag{2}$$

These equations would be most useful when the jets start blowing as the flow would re-laminarize.

Without the activation of jets, the flow separates after the onset of turbulence. For turbulent boundary layers, there is mean flow and fluctuating flow. Mean flow is represented by $\bar{u}$ and the fluctuating component is represented by u', as demonstrated in [4]. The major condition for turbulence being $Re >> 1$ implies that

$$\delta(x) << x$$

$$\frac{\partial}{\partial x} << \frac{\partial}{\partial y}$$

As shown in [5], the continuity equation would simplify to:

$$\frac{d\bar{u}}{dx} + \frac{d\bar{v}}{dy} = 0 \tag{3}$$

Each tube of jet, which has an Re of approximately 700 can be considered as laminar. The jets obviously do not create a pressure gradient and have constant momentum flux due to the absence of bounding walls. Nonetheless, there is entrainment.
Momentum flux, given by J is considered to be constant as demonstrated in [4] and [5] by the following equation:

$$J = \rho \int u^2 dy = constant$$

Now observing the jets which blow tangentially, we have certain conditions for the boundary layer.
The velocity $u_w > 0$ (as opposed to suction where $u_w < 0$) and we know that in any B.L. with blowing would yield: $u_w >> v$.

Schlichting *et al* [6] gives the required equations to simplify the net momentum equation to:

$$\rho u_w \frac{\partial u_w}{\partial y} \approx \frac{dP}{dx} \frac{\partial \tau}{\partial y} \tag{4}$$

where τ is defined as follows:

$$\tau - \frac{du}{dy}$$

In the later section we'll understand the quantification of pressure gradient, but using the previous equation, we can elementarily estimate it to be the magnitude of:

$$\rho u_w \frac{\partial u_w}{\partial y} - \nu \frac{d^2 u}{dy^2} \tag{5}$$

The momentum of the jets have to be greater than the momentum created by the back flow due to the pressure gradient. As a result, the equation theoretically shows the restoration of the boundary layer and laminarity of flow due to the low Re of the jets.

2.2 Transition to turbulence

The jets are inclined towards the x-axis instead of the y-axis making them more effective than the general case of blowing. The Re of each tube of the jet approximates to 700 by understanding turbulent jets [7], implying laminar flow. Granville's method of determining the length between beginning point of instabilities x_i and transition x_{tr} can theoretically demonstrate the laminarity of flow till the tail of the airfoil.

$$\lambda_m = \frac{1}{x_{tr} - x_i} \left(\int_{x_i}^{x_{tr}} \lambda(x)\, dx \right) \tag{6}$$

where λ is defined as follows:

$$\lambda = \theta^2 \frac{dU}{dx} / \nu [10$$

Granville also obtained the relation $Re(x_{tr}) \approx Re(x_i) + 450 + 400e^{60\lambda_m}$ for $\lambda < 0.04$ as given in [5].

For an adverse gradient, $\lambda \approx -0.1$ showing that the x_i and x_{tr} are close. With blowing jets, λ_m can get very large, due to the lack of an adverse gradient, as a favourable gradient is created, implying that x_i and x_{tr} are far apart. This will be empirically tested and proven in the subsequent sections.

2.3 Pressure Gradients

Previously we understood a basic approximation for the pressure gradient. Now, we can go further into the understanding of pressure gradients without any blowing.

We find that the adverse pressure gradient of laminar flow still affects the flow separation before its transition to turbulence as well as during the turbulent flow. This is because the turbulent mixing wouldn't create enough momentum of the flow to combat the large pressure gradient created.

The Karmen-Polhausen method is applied to determine the nature of the adverse pressure gradient causing the separated flow: In Polhausen's method,the parameter λ is has a value of -12

.

Using Prandtl's modified version of Polhausen's parameter, we take -10 as the ideal λ value, which is explained by Paul K Chang [8]. From Polhausen-Karmen equations, we get:

$$\lambda = \frac{\delta^2}{\nu} \frac{dU}{dx} = -\frac{dP}{dx} \frac{\delta^2}{\mu U} = -10 \tag{7}$$

We get the pressure gradient magnitude $\left|\frac{dP}{dx}\right|$ as $10 \left|\frac{\mu U}{\delta^2}\right|$.

Prandtl, after equating Polhausen-Karmen's equations, used another parameter to determine flow separation, which reads as follows:

$$\sigma = \frac{U \frac{d^2 U}{dx^2}}{\left(\frac{dU}{dx}\right)^2} \tag{8}$$

If $\lambda = -10$, we can equivalently determine that $\sigma \approx 11$. These are the values for the flow to avoid separation.

Prandtl further calculated the potential velocity relation with distance in the following function derived from (7) shown in [8]:

$$U(x) = \frac{U_0}{(1 + 10c_1 x)^{\frac{1}{10}}} \tag{9}$$

Using boundary layer thickness equations, we find:

$$c_1 = \frac{10\nu}{U\delta^2}$$

This is the velocity for which separation can be avoided. We therefore conclude that the parameter we've rendered is perfect for measuring the minimum adverse pressure gradient so that flow won't separate. That would give us the ideal momentum of jet needed. The pressure gradient and potential velocity are interchangeable with the following relation:

$$\frac{dP}{dx} = -U(x) \frac{dU}{dx}$$

The pressure gradient derived from this relationship converges towards $x^{\frac{-6}{5}}$ which is obviously > 0 at all values of x.

x is the distance downstream from the separation point. The flow is mostly laminar before separation. This is contrary to the fact that adverse pressure gradients initiate the transition early because the angle of attack is beyond stalling, but looking at the formula $Re_x = \frac{Ux}{\nu}$ [4], the flow seems to have laminar properties for the most part before separation.

It is also accurate that $dP/dx > 0$.

The jets eliminate the pressure gradient near the rear stagnation point and the constant high velocity of the jet v_w ensures that the it is shifted, hence the pressure becomes lesser.

3 Experimental Verification

Testing the hypothesis rendered from the theoretical analysis above is an important goal of this paper. The impact of blowing jets for the re-attachment of airflow over the wing surface was verified using low-cost imagery apparatus and processing methods. Furthermore, the wing-section was modified with blowing jets on its upper surface using cost-effective resources and scrap material. The following subsections elaborate on each of the experiment's aspects:

3.1 Windtunnel Setup

Testing the impact of the blowing jet was conducted in a low-speed open-circuit blow type windtunnel, modified to accommodate an active airfoil. Fig. 1 depicts the apparatus' construction. The labelled parts are described below:

1 - the contraction cone directs the air into the tunnel, speeding it up due to the difference in inlet and outlet apertures; optimisations were taken from Mehta and Bradshaw [9].

2 - shows the honeycomb flow straightener, designed to remove turbulence from the incoming air.

3 - the test section constructed with transparent acrylic to allow total observation.

4 - labels the diffuser, a component designed to gradually allow pressure recovery necessary to the flow quality in the test section. The dimensions for which are taken from Bradshaw and Pankhurst [10].

3.2 Imagery-Data Capture

Transparent test section construction allowed the camera setup demonstrated in fig. 2 to capture imagery produced from the airfoil's interactions. 1 - the high frame rate camera was calibrated to extract true-color images of the streamlines flowing over the airfoil; 2 - the frame section was utilised as the plane of reference to make all observations.

Aerodynamic interactions are made visible by the flow visualiser which injects opaque CO_2 onto the regions of interest.

3.3 Sanctity Testing the Apparatus

Since the project utilised scratch-built equipment, pre-testing conditions of the windtunnel were verified to be conducive to conduct replicable research. Motion-tracking analysis deduced that there was an ideal streamlined flow in the test section. An average spatial render of fluid particle position plots reveals that the fluid flow of the test section is laminar in nature.

3.4 Blowing jet mechanism

Experimental verification required the construction of a modified scaled-down wing section with the NACA 2412 airfoil. The modified airfoil incorporates a Trailing Edge Blowing (TEB) construction the nozzle jet surfacing at 0.85 the length of the chord. Gerhard *et al* [11] show the construction of TEB airfoils, with trip numbers 82.5 referring to orientations similar to the single piece airfoil utilised in the experiment.

Sillicon tubes (5mm), which remains in the prescribed $1\% - 5\%$ of the chord length in diameter, is implanted through the wing onto its upper face. These serve as dispensers for the jet stream designed to blow across the wing surface. The TEB orientation of the jet was placed at an inclined angle (α_{jet}) of 0° The ratio between the coefficient of lift to the co-efficient of drag - C_l to C_d - was found to be at its absolute maxima at the inclined angle of 0°. Monir and Bakhitan [12] demonstrate that the highest $C_l/C_d = 11.19$ value was found at $\alpha_{jet} = 0^\circ$ for a NACA 0012 airfoil. Furthermore, the blowing velocities were approximately set to the values derived from relation (9) in section 2.3 of this paper.

The jets were powered by an individual power pod. fig. 3 demonstrates the modified build. 1 - depicts the construction method designed to influence the upper wing surface. 2 - shows the x component orientation of the jet.

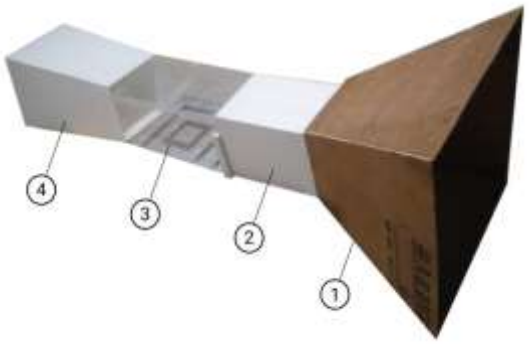

Fig. 1: Scratch-built open-circuit Wind tunnel apparatus

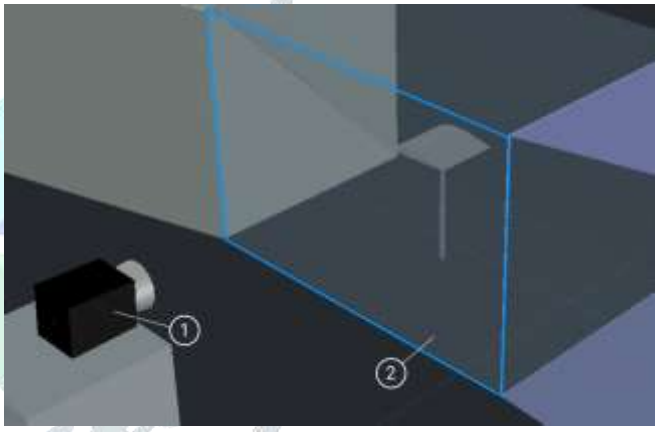

Fig. 2: Streamline Imagery Experimental Data Setup

Fig. 3: TEB Modified NACA 2412 Airfoil
(a) Modified Test Section Inlet - Blowing Tubes
(b) Blowing jet lateral orientation $\alpha_{jet} = 0^\circ$

The orientation of the jets, as specified in section 2, is designed to contribute primarily to the fluid velocity in the x component. Tangentially blowing the jet is predicted to curtail the early separation of flow. Low-cost material, tubes/etc., were utilised for the experimental setup of the blowing jets.

4 Fluid Pathline Plotting Method for Airflow's Nature Determination

The plots of the path traversed by an arbitrary fluid particle have been rendered from the outline of the observable streamline. An array of image processing methods were utilised for the conversion of images into data relevant to the analysis of the boundary layer. The algorithm is explained in the following sub-sections in this exact order:

4.1 Greyscaling

The original image is computed to highlight all pixels fitting in the RGB chromatic range of the observable streamline. For the first step of classifying pixels as potential streamlines points, the colors of the image's pixels are compared with a color range of the fluid-stream. This moulds a probabilistic two-class classification problem.

Let c be the color feature vector of a pixel, s be the streamline's color class. The experimental imagery processing of this research uses a modified method of color detection used by Liu *et al* [13] that defines a set containing the range of colors values that represent the chromatic range of the opaque streamline in the windtunnel. The posteriori probabilities of streamline colors and non-streamline colors as $P(s|c)$ and $P(s|c)$ respectively. Based on the Bayesian decision for minimum error rate, a pixel should be classified as a streamline path if:

$$P(s|c) > P(s|c)$$

wherein the selected pixel is considered to be part of the chromatic range of the streamline:

$$if P(s|c) = \frac{p(\mathbf{c}|s)P(s)}{p(\mathbf{c})} > 0.5, then \quad \mathrm{c} \in s \tag{10}$$

The component intensitites of each chromatic value in the RGB-axes is given by the following:

$$r = \frac{R}{(R+G+B)}, g = \frac{G}{(R+G+B)}, b = \frac{B}{(R+G+B)} \tag{11}$$

On a digitised scale of 0-255, the individual color intensities (R, B, and G) were mapped on the 3 dimensional graph using (11).

The final processing occurs on the greyscale, the distance component that yields the general intensity of the chromatic output. Colors that don't fit the (x,x,x) co-ordinates are evaluated by projecting onto the greyscale line. The RGB component definitions and greyscaling are demonstrated in Dwairi *et al* [14].

The targetted grayscale range s that contains the opaque streamline is manually derived from the image; the regions matching those chromatic indices are marked and further processed, producing the clearest possible image of the fluid path. The comparison between an original image and a greyscaled one is presented in fig. 4:

Fig. 4: (a) Original Image
(b) Greyscaled by projection method

4.2 Fluid Path Plotting

The fluid path made visible by the processing is traced along its visible boundaries. In cases of dispersed fluid clouds, the outermost boundaries are selected and are usually characterised as separated/turbulent compared to their coalesced counterparts that do not contain dispersed fluid particles between their boundaries.

4.3 Corrections

Plot points are corrected for parallax and other errors. The points obtained on overlaying the original co-ordinates obtained from the experiment are posted on a corrected *xy* plane.

4.4 Graphical Analysis

The corrected points are then plotted graphically, replicating the position co-ordinates that trace the streamline from the previous step. These graphs plot the upper and lower layers of the streamline, containing data regarding their thickness and shape from which we imply their nature.

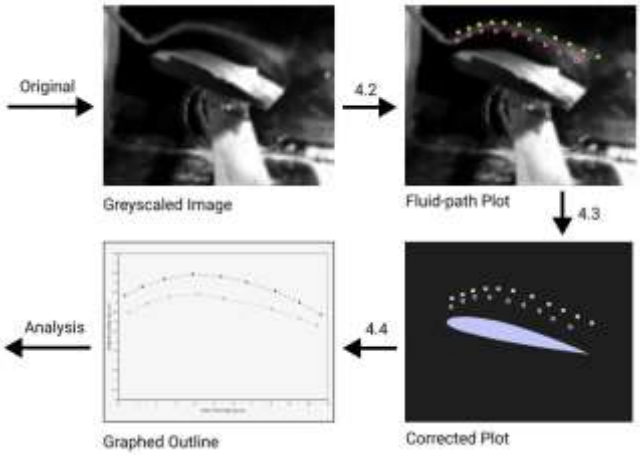

Fig. 5: Streamline Plotting Method Process Diagram

5 Experimental Results

The qualitative verification method utilised in this paper builds on imagery analysis conducted in wind tunnel testing of aerodynamic prototypes. While Zhulev and Inshakov [15] used the smoking wire technique to qualitatively demonstrate the attached-flow properties of a tangential-blowing method, they utilise standard parametric data to verify the gross improvement to airflow their model yields. This paper exclusively uses fluid path plots and streamlines to determine the qualitative state of the airflow.

The utilisation of imagery as direct confirmatory evidence is a relatively unique approach, which, by implication of the works of Zhulev *et al* [16], Fatahian *et al* [15], etc. accurately points towards the quantitative meaning of improved airflow.

The image renders from advanced CFD techniques including large-eddy simulations (LES) support the implications of higher flow qualities with streamline imagery that demonstrates an attached boundary layer which occurs on blowing. You and Moin [1] computationally verify the laminar imagery obtained by Gilarranz *et al* [17] upon blowing across wing surfaces. Therefore, the experimental results of this testing method appropriately fulfills the qualitative scope of this study.

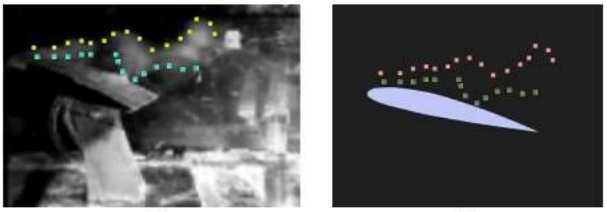

(a) (b)

Fig. 6: (a) Fluid Path line Plot - Greyscaled Image(b) Corrected *xy* Path line position-plot (NACA 2412)

5.1 Separated Flow Path Data

The analysis of the flow-plots over the surface of the airfoil at high angles of attack captures the boundary-layer's nature.

Frame-by-frame imagery demonstrates the formation of a vortex around the vicinity of the trailing edge of the airfoil.

Upon rendering the points on a corrected *xy* plane, the derived plot reveals an irregularly shaped fluid dispersion, indicating separation of flow and formation of turbulent wakes and eddies. Besides the average distance between the upper and the lower layer, which is indicative of the stream's thickness, the irregular shape of the fluid path curves suggests the lack of laminarity.

The process was repeated for a series of frames to procure an accurate characteristic of the flow. Fig. 6 demonstrates the corrected image from the greyscale plot. This render determined that the plot bore an irregular shape and the airflow was therefore turbulent. Repeating the process to produce true pathlines for the de-activated jet regime over the angled wing is shown in fig. 7(a).

6 Activated Jet - Data Comparison

Upon the activation of synthetic jets under similar conditions, the airflow has become more coalesced with the surface of the airfoil. We notice that the thickness is far less than the fluid cloud produced due to the separated flow in fig. 6(a). It was not necessary to alter the fluid stream velocity, since Duvigneau and Visonneau [18] suggest that as the α increases to a point beyond the stall angle, $18^\circ - 22^\circ$, the jet velocity doesn't require incrementation. Huang *et al* [19] also notes a similar result. The single jet velocity therefore produced similar laminarity effects for the velocities tested.

Plots rendered from the wing section with the synthetic jets activated under the exact conditions of freestream velocity and α reveal the formation of a laminar fluid-stream that traces the airfoil's shape. A regular upper and lower boundary of the fluid path sketch shows similarly shaped curves in the graph fig. 7(b), indicative of an improved airflow quality. Furthermore, the indication of x_i and x_{tr} are appropriately demonstrated in the obtained plots, referencing section 2.2 of this paper.

The flow velocity passing through the jet of the order $80\% - 100\%$ of the freestream velocity v_x contributes to the velocity profile over the wing's surface. The nature of the jets close to the airfoil's surface produces remarkable effects in removing the turbulent fluid flow and re-attaching the boundary layer [2].

If a jet is positioned close to a surface, pressure forces change the path of the fluid elements. Thus the jet is deflected to the surface and becomes a tangential wall jet. Pfingston *et al* [2] further demonstrate that the flow in the vicinity of the jet is accelerated by virtue of the coanda-effect, and since the wall prevents fluid inflow into the area between the jet and the wall, pressure decreases.

(a)

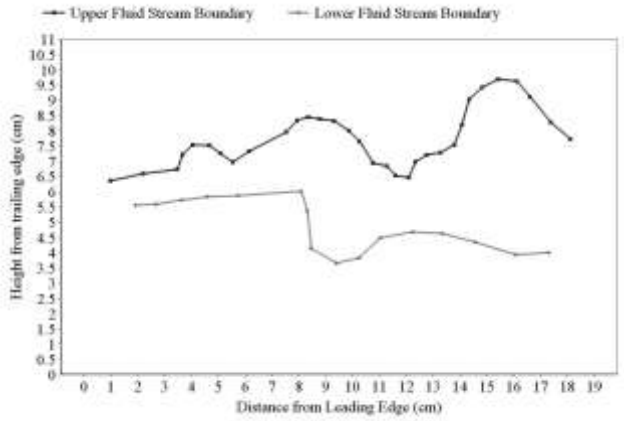

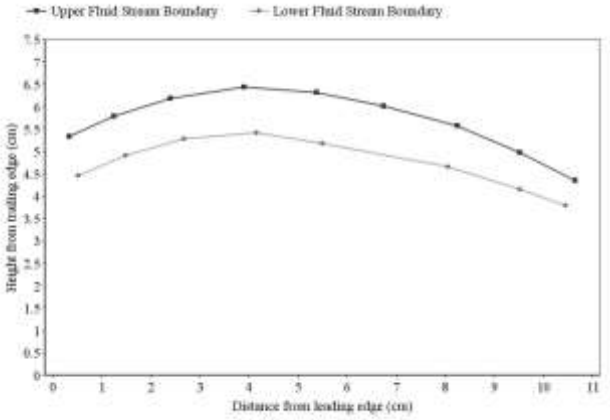

(b)

Fig. 7: (a) Path line Position Plot - De-activated Jets (Separated Flow Conditions) (b) Path line Position Plot - Activated Jets

Modelling the pressure gradient in two dimensions, we note the following analysis:

$$u\frac{\partial u}{\partial x} + v\frac{\partial u}{\partial y} = -\frac{1}{\rho}\frac{\partial p}{\partial x} + v\frac{\partial^2 u}{\partial y^2} \tag{12}$$

The activated jets contribute to the local velocity vectors u,v thereby incurring a reduction in the severity of the pressure gradient, as observed from the equation (12) - this builds on the relation obtained in equation (7). The flow's coalescence and laminarity markedly improve with the onset of jet activation.

A comparison between the two plots demonstrates the difference in flow quality. The activated jets produce a plot that demonstrates the qualitative improvement of airflow as shown by the experiment we've constructed.

7 Conclusion

The primary objective of this paper is to demonstrate that lowcost apparatus and methods can effectively demonstrate marked improvements in fluid flow that arise from active tangential blowing. This method of testing which utilises streamline plots based on direct imagery data is one of the more cost-effective

methods of demonstrating fluid characteristics. You and Moin, for example, conduct resource-heavy LES and other Computational Fluid Dynamics (CFD) simulations with about 8 and 15 million cells [1]. Circumventing those costs, the method propogated in this paper's experimental verification feasibly demonstrates realistic non-simulatory fluid flow paths.

Keen and Mason [20] also verified their theroetical hypotheses using experimental results of a 2D plot methodology. The imagery method in this paper is a similar attempt at characterising fluid flow.

This experimental method proved that by eliminating the pressure gradient of back-flow, the flow was smooth and separation of the flow was negligible. The graphs displayed the laminar properties of the jets (verifying Granville's equation and the Re formula) and induced laminarity of the flow during blowing. The process rendered Pathline plots that demonstrates the re-laminarised airflow on the activation of the blowing jets.

References

[1] You D and Moin P 2008 Active control of flow separation over an airfoil using synthetic jets. J. Fluid Struct. 24: 1349–1357

[2] Pfingsten, Kai C., and Rolf Radespiel. "Experimental and numerical investigation of a circulation control airfoil." 47th AIAA Aerospace Sciences Meeting (2009).

[3] A. Prabhakar, "CFD Analysis on MAV NACA 2412 Wing in High Lift Take-Off Configuration for Enhanced Lift Generation," Journal of Aeronautics Aerospace Engineering, vol. 02, no. 05, 2013.

[4] Kundu, Pijush K., Ira M. Cohen, and Howard H. Hu. 2004. Fluid mechanics.

[5] White, Frank M. 1974. Viscous fluid flow. New York: McGraw-Hill.

[6] Schlichting, Herrmann, and Klaus Gersten. Boundary-layer theory. Springer Science and Business Media, 2003.

[7] Lee J.H.W., Chu V.H. (2003) Turbulent Jets. In: Turbulent Jets and Plumes. Springer, Boston, MA. https://doi.org/10.1007/978-14615-0407-82

[8] Chang, Paul K. Separation of flow. Elsevier, 2014.

[9] Mehta, R., and Bradshaw, P. (1979). Design rules for small low speed wind tunnels. The Aeronautical Journal (1968), Volume 83, 443-453. doi:10.1017/S0001924000031985

[10] P. Bradshaw, R.C. Pankhurst. The design of low-speed wind tunnels. Progress in Aerospace Sciences (1964), Volume 5, 1-69. https://doi.org/10.1016/0376-0421(64)90003-X

[11] Gerhard, T and Erbsloeh, Sascha and Carolus, Thomas. (2014). Reduction of airfoil trailing edge noise by trailing edge blowing. Journal of Physics: Conference Series. 524. 012123. 10.1088/17426596/524/1/012123.

[12] H. Esmaeili Monir, M. Tadjfar, A. Bakhtian, Tangential synthetic jets for separation control, Journal of Fluids and Structures, Volume 45, 2014, https://doi.org/10.1016/j.jfluidstructs.2013.11.011.

[13] Liu, Leyuan Sang, Nong Yang, Saiyong Huang, Rui.
(2011). Real-Time Skin Color Detection under Rapidly Changing Illumination Conditions. IEEE Transactions on Consumer Electronics - IEEE TRANS CONSUM ELECTRON. 57. 1295-1302. 10.1109/TCE.2011.6018887.

[14] Dwairi, Majed Alqadi, Ziad Abujazar, Amjad Abu Zneit, Rushdi. (2010). Optimized True-Color Image Processing.

[15] Zhulev, Y.G., Inshakov, S.I. On the possibility of enhancing the efficiency of tangential blowing of a slit jet from an airfoil surface. Fluid Dyn 31, 631–634 (1996). https://doi.org/10.1007/BF02031774

[16] Fatahian, E., Lohrasbi Nichkoohi, A., Salarian, H. et al. Comparative study of flow separation control using suction and blowing over an airfoil with/without flap. Sadhan¯ a 44, 220 (2019).¯

[17] Gilarranz, J. L., Traub, L. W., and Rediniotis, O. K. (May 10, 2005). "A New Class of Synthetic Jet Actuators—Part II: Application to Flow Separation Control ." ASME. J. Fluids Eng. March 2005; 127(2): 377–387. https://doi.org/10.1115/1.1882393

[18] Duvigneau, Régis Visonneau, Michel. (2006). Simulation and Optimization of Stall Control for an Airfoil with a Synthetic Jet. Aerospace Science and Technology. 10. 279-287. 10.1016/j.ast.2006.01.002.

[19] Huang L, Huang P G, LeBeau R P and Hauser T 2004 Numerical study of blowing and suction control mechanism on NACA0012 airfoil. J. Aircraft 41: 1005–1013

[20] Keen, Ernest Mason, William. (2005). A Conceptual Design Methodology for Predicting the Aerodynamics of Upper Surface Blowing on Airfoils and Wings. 10.2514/6.2005-5216.

[21] Landau, L. D. and Lifshitz, E. M.. Fluid Mechanics, Second Edition: Volume 6 (Course of Theoretical Physics). 2 : ButterworthHeinemann, 1987.

8 Appendices

Eddies:

It is not necessary to analyse eddies, but we can understand that the presence of large eddies in the experiment is proof of high Re. In Landau and Lifshitz's work [21], it is explained that over large distances where the Re is high, the variation of fluctuating velocities is given by the variation of velocity of large eddies and is comparable with Δu. We can define a Reynolds number for large eddies $R \sim v_\lambda \lambda / \nu$

For these kinds of large eddies, the viscosity is negligible. So we can instead define another viscosity term, the turbulent viscosity ν_{turb} which is of magnitude $l\Delta u$. Consequently, we get $\frac{\nu_{turb}}{\nu} \sim Re$

During the entire experiment, we observed the energy and internal ranges of λ: $\lambda \sim l$ and $\lambda_0 << \lambda << l$.

These observations could be useful for future work involving drag and lift.